Monatshefte für Chemie 137, 1487–1498 (2006)
DOI 10.1007/s00706-006-0552-7

Monatshefte für Chemie
Chemical Monthly
Printed in Austria

Non Aqueous Titration and Catalytic Conversion of Cyclohexanol as a Test of Surface Acidity

El-Sayed A. El-Sharkawy[*,#]

Chemistry Department, College of Education at Al-Arish, Suez Canal University, Al-Arish, Egypt

Received March 12, 2006; accepted September 10, 2006
Published online November 9, 2006

Summary. The textural characteristics, including surface area, mean pore diameters, and total pore volume of Cr_2O_3–CuO/Al_2O_3 solid catalysts were determined from the low temperature adsorption of N_2 at 77 K. The structural properties were investigated using XRD. The surface acidity of calcined samples was determined using two comparable methods, including the non-aqueous titration of acidic groups with *n*-butylamine and dehydration/dehydrogenation activity of cyclohexanol.

XRD patterns assigned a crystalline CuO and γ-Al_2O_3 for 723 K calcinations products of lower Cr_2O_3 content. The gradual increase of calcinations temperature promoted the crystallinity of Cr_2O_3 and resulted in solid–solid interaction of CuO and Cr_2O_3 forming $CuCr_2O_4$. The textural parameters varied with both calcinations temperature and catalyst composition. The surface acid density (DAS) increased with the increase of chromia content up to 0.132 mole% Cr_2O_3, while the rise of calcinations temperature led to a decrease of surface acidity.

The dehydration/dehydrogenation of cyclohexanol as well as *n*-butylamine titration succeeded in characterizing of surface acidity.

Keywords. Al_2O_3; Cr_2O_3; CuO; Magnetic susceptibility; Surface acidity.

Introduction

Surface acidity of catalysts was approved as a motivating power in many industrial processes, *e.g.* dehydration of various alcohols, polymerization of unsaturated compounds, isomerisation, cracking, and hydrocracking. The surface acidity can be measured through the use of a variety of techniques. Among these methods may be cited the titration of catalysts with *n*-butylamine in the presence of *Hammett* indicators [1, 2], microcalorimetric methods and infrared spectroscopy [3, 4],

* E-mail: easharkawy@yahoo.com
# Present address: Chemistry Department, College of Science, King Faisal University, Al-Hofuf 31982, Saudi Arabia

temperature programmed desorption (TPD) of adsorbed bases [5–7], using of DTA and TGA [4, 8], and poisoning of acid centers with some organic bases [9, 10]. In addition, the dehydration of aliphatic and alicyclic alcohols has been used as an alternative method for the characterization of surface acidity–basicity [11–13]. The latter method is convenient because it enables the determination of acidic characters during the reaction performance. Indeed, studies of the acid–base properties of solid catalysts become of increasing importance as a means of directing the reaction pathways, *i.e.* in increasing the selectivity towards particular products.

Moreover, the measured textural properties of solid catalysts, namely specific surface area, pore structure, and total pore volume, makes more or less significant contribution to the catalytic properties. Such surface characteristics were affected by a number of variables, *viz.* metal content, methods of preparation, type of support, and pre-thermal treatments [11, 14–20]. The correlation between surface and structural characteristics of ternary solid catalysts should be the aim of investigations in applied surface science prospects. However, there are few reports studying the physico-chemical properties of Cr–Cu–Al–O system and their uses in the catalytic conversion of alicyclic alcohols.

The ultimate goal of this research concerned with finding a simple and comparable method to determine the surface acidity *via* the non-aqueous titration of acidic groups with *n*-butylamine and dehydration/dehydrogenation activity of cyclohexyl alcohol. Indeed, studying how the different reaction parameters can control the course of reaction pathway. The use of cyclohexyl alcohol for this concern was arisen from: (i) the reaction produces on an aliphatic cyclic ketone, namely cyclohexanone as precursor of Nylon-6; (ii) the reaction can be used to differentiate between the acidity of various solid catalysts.

Results and Discussion

Powder X-Ray Diffraction (XRD)

Figure 1 shows XRD patterns of the calcined Cr–Cu–Al–O samples. The products of chromia content up to 0.066 mole% calcined at 723 K revealed a well crystalline CuO and γ-Al_2O_3. The XRD lines corresponded to CuO at 2θ values of 35.6, 38.7, 48.8, and 68°, whereas γ-Al_2O_3 centered at XRD lines of 32.6, 44.8, 62.5, and 66.2° [5, 23]. The particle size of CuO in the calcined samples containing 0.033 and 0.066 mole% Cr_2O_3 was estimated as 119.0 and 34.0 nm, respectively. The change of particle size resulted in variation of textural parameters. The progressive increase of mole% chromia within of 0.099–0.230 inhibited the crystallinity of both copper oxide and aluminum oxide and therefore led to the formation of an amorphous matrix. However, the ramps of calcinations temperature up to 923 K enhanced the crystallinity of all samples, the catalysts of 0.033 mole% chromia didn't show any spinel formation while CuO was the only detected phase. The disappearance of XRD lines specified for chromium oxide or other chromium spinel may be rationalized to, firstly, the highest dispersion of chromium precursor on the high surface area of alumina, particularly at lower Cr(III) content. Secondly, in co-impregnating of Cu^{2+} and Cr^{3+} precursor into $Al(OH)_3$, chromium(III) nitrate was strongly adsorbed and deposited on the alumina surface, while copper(III) nitrate was less adsorbed and penetrated into alumina

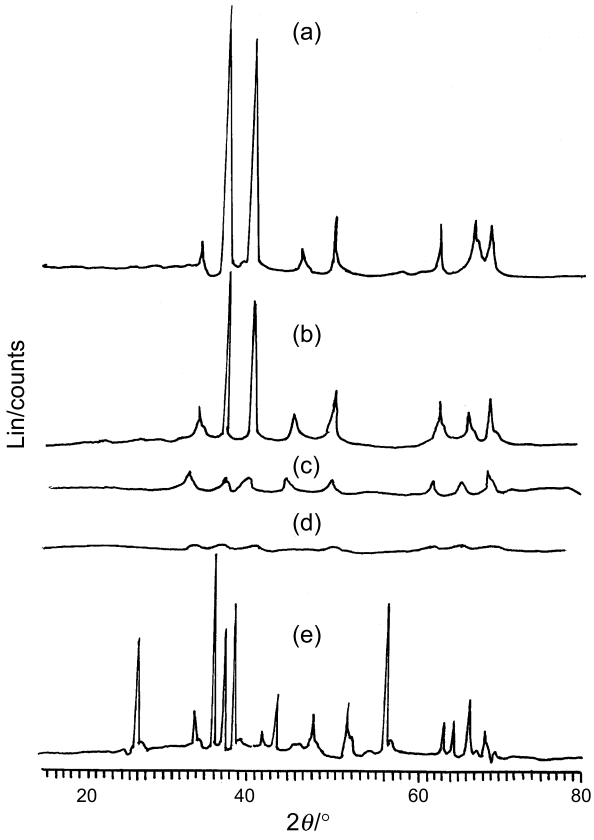

Fig. 1. XRD patterns of: (a) AcuCr1-I, (b) AcuCr2-I, (c) ACuCr3-I, (d) ACuCr4-I, and (e) AcuCr4-II catalysts

matrix [24]. The patterns of calcined samples containing 0.099–0.230 mole% Cr_2O_3 was also investigated, where γ-Al_2O_3 and copper chromite ($CuCr_2O_4$, $2\theta = 35.29$ and 37.7°) of crystallite size 9.0–47.0 nm were assigned. The latter phase indicated solid–solid interaction between CuO and Cr_2O_3. The addition of 0.099–0.23 mole% Cr_2O_3 to Cu–Al–O system led to a disappearance of all diffraction CuO characteristic peaks. This may indicate that Cr_2O_3 – doping of examined catalysts decreased crystallite size of CuO beyond the detection limits of X-ray diffractometer. In other word, the doping process increased the degree of dispersion of CuO phase.

The progressive increase of chromia content, particularly at the calcination temperatures $\geq$923 K, led to crystallization of Cr_2O_3 ($d \approx 128.8$ nm) at 2θ of 24.5, 33.5, 36.2, 41.4, 50.2, 54.8, 63.5, and 65° [25]. In brief, the rise of calcination temperature promotes the crystallization of Cr_2O_3 and $CuCr_2O_4$. The change of XRD patterns is due to structural transformation from the amorphous or disordered into crystalline form and thereby resulted in a significant change of surface characteristics.

Textural Properties Measurements

The adsorption of nitrogen at 77 K on all investigated catalysts was found to be rapid, assuming the absence of ultra fine pores. According to BDDT classification

[26], the adsorption of N_2 over products calcined at 723 K exhibited type II isotherms and type IV was observed for products calcined at temperatures exceeding 723 K (Fig. 2). This indicated the creation of some mesopores with the progressive

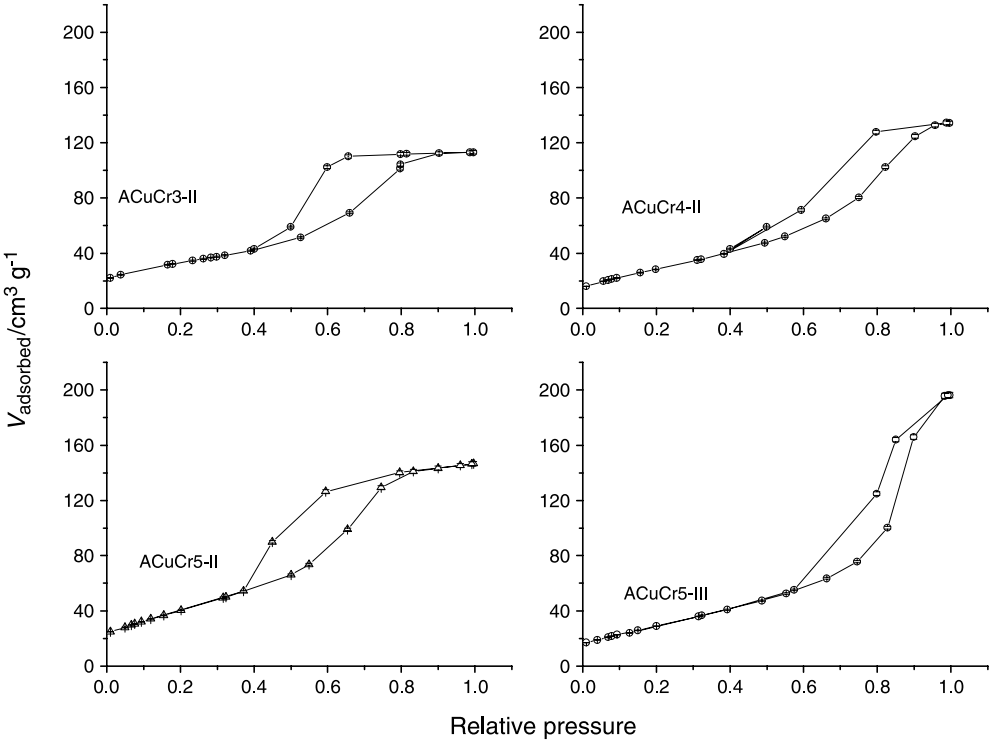

Fig. 2. Adsorption-desorption isotherms of N_2 at 77 K over some selected samples

Table 1. Textural parameters obtained from N_2-adsorption at 77 K

Sample	S_{BET} (m^2/g)	V_T (cm^3/g)	R_P (nm)	ΔE_1[a] 723–923 K	ΔE_2[b] 923–1123 K
ACuCr1-I	25.4	0.025	19.7	20.0	−23.2
ACuCr2-I	33.7	0.048	23.7	15.6	−19.0
ACuCr3-I	39.6	0.050	25.2	24.9	−35.4
ACuCr4-I	44.1	0.058	26.3	24.4	−21.7
ACuCr5-I	53.7	0.078	25.0	28.3	−14.0
ACuCr1-II	52.3	0.106	40.5		
ACuCr2-II	59.2	0.127	42.9		
ACuCr3-II	97.0	0.214	44.1		
ACuCr4-II	106.4	0.257	48.3		
ACuCr5-II	148.7	0.374	50.3		
ACuCr1-III	30.5	0.094	61.5		
ACuCr2-III	38.1	0.122	64.2		
ACuCr3-III	42.7	0.143	67.1		
ACuCr4-III	64.3	0.230	71.6		
ACuCr5-III	107.4	0.400	74.5		

[a] ΔE_1 is the activation energy of activation phenomena, [b] ΔE_2 is the activation energy of the sintering process

increase of temperature. The adsorption and desorption branches met at intermediate relative pressure of 0.4–0.5, giving closed hysteresis loops of type A [27, 28]. The change of isotherm shapes may be related to the direct dependence of porous texture on the thermal treatments of catalysts and/or the chemical composition [11, 25].

The adsorption isotherms enabled us to estimate the specific surface area (S_{BET} (m^2/g)), the total pore volumes (V_T (cm^3/g)), and the mean pore radii (R_P (nm)) of the catalysts investigated (Table 1).

Inspection of Table 1 reveals that: (i) For the same calcination temperature, the specific surface area increased with the continuous increase of chromium content. The change of S_{BET} was much more pronounced for the calcinations products at 923 and 1123 K. For 723 K-calcination products, our assignments for XRD patterns demonstrated the inhibition of catalyst crystallinity upon increasing chromia content, causing thus an increase of S_{BET} values. (ii) The rise of calcination temperature from 723 to 923 K developed the porosity of catalysts and resulted in an increase of S_{BET}. Further elevation of thermal treatment up to 1123 K led to a partial collapse of porous structure, reducing thereby the total pore volume and increasing the mean pore radius. In the course of thermal treatment of a solid, two processes operate, namely activation at relatively low temperature to create new pores and sintering at higher temperatures. Sintering phenomena were associated with increasing particle-particle interaction and subsequent adhesion, leading to pore widening, a decrease in the number of micropores, and a consequent lowering of specific surface area [29–31].

The calculated activation energies (ΔE) of both processes throw light on the dependence of the porous texture of the investigated catalysts on their structural properties. ΔE was evaluated using the values of S_{BET}-N_2 data, adopting the relationship shown in Eq. (1) [32, 33] where A is a constant and ΔE the approximate value of activation energy.

$$S_{BET}\text{-}N_2 = A\, e^{-\Delta E/RT} \tag{1}$$

When the surface area within a definite range of temperatures was used, the values of ΔE could be calculated according to Eq. (2).

$$2.303\,R\ \log (S_{BET})_{T_2}/(S_{BET})_{T_1} = -\Delta E(1/T_2 - 1/T_1) \tag{2}$$

The calculated activation energies depicted a general increase of ΔE_1 within the temperature range of 723–923 K, where a significant increase of S_{BET}-N_2 was observed. This may be attributed to the development of new pores with the continuous increase of % chromium contents, *via* the earlier stage of thermal treatment, *i.e.* activation process. In other words, the adsorbed species of Cr(III) hindered the activation ability within the temperature range of 723–923 K, causing an increase of ΔE_1. The higher thermal treatment, up to 923–1123 K gave lower values of ΔE_2 compared with ΔE_1. XRD analyses matches to a great extent the variation of the measured textural parameters. During the course of higher thermal treatment beyond 923 K, sintering of solid led to particle–particle adhesion, grain growth, and collapse of the porous texture. The increase of ΔE_2 may be explained from the role of Cr_2O_3 in hindering the sinter-ability of investigated systems.

Figure 3 shows representative BJH differential pore volume distribution curves of ACuCr4-II. The maxima of pore volume increase upon elevating the calcination

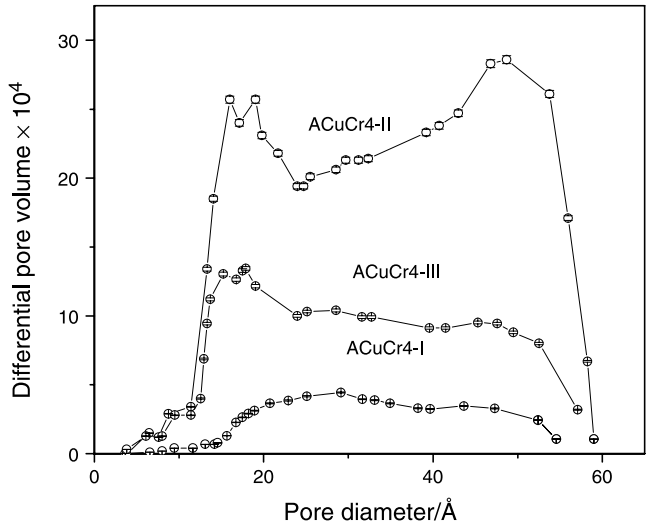

Fig. 3. Pore volume distribution curves of some calcination product samples

temperature from 723 to 923 K, while their position was shifted to higher pore width with more contribution of micro pores. The peak maxima were reduced upon exceeding the temperature to 923 K, attributing to the partial disappearance of micropores and creating some wider pores.

Surface Acidity Measurements

Figure 4 illustrates the change of electrode potential with the continuous addition of *n*-butylamine. It is evident that the electrode potential decreases with the progressive neutralization of acidic surface sites until the inflection point, where no remarkable change of the electrode with further addition of titrant occurs. The inflection point related to the volume of *n*-butylamine required to neutralize

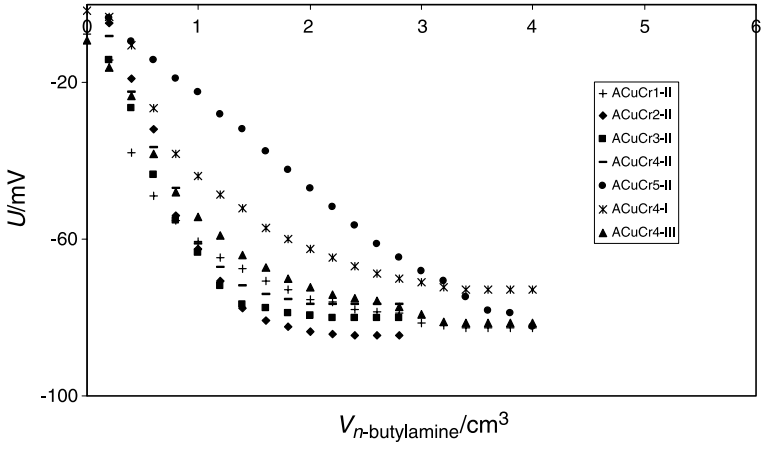

Fig. 4. Acidity titration curves of pre-calcined investigated catalysts

Table 2. Surface acidity and μ_{eff} of investigated catalysts, conversion, S_{DHD}, and S_{DHG} of cyclohexanol

Sample	Conversion (%)		Selectivity (%)		Acid amount ($N_{acid\ sites} \times 10^{-21}$)	μ_{eff}
	DHD	DHG	S_{DHD}	S_{DHG}		
ACuCr4-I	5.2	22.0	19.1	80.9	10.08	1.28
ACuCr1-II	10.5	33.9	23.6	76.4	5.12	0.73
ACuCr2-II	18.8	38.1	33.0	67.0	6.09	0.77
ACuCr3-II	27.4	42.5	39.2	60.8	7.43	1.48
ACuCr4-II	33.1	47.5	41.1	58.9	23.15	1.50
ACuCr5-II	15.8	49.1	24.3	75.7	8.77	1.58
ACuCr4-III	15.9	26.9	37.1	62.9	7.45	1.31

completely the surface acid sites. Assuming each acid site can be probed by one molecule of *n*-butylamine, the density of surface acid sites (DAS) were estimated. Listed in Table 2 are the values of DAS for the 923 K-calcined samples, while the DAS of ACuCr4-I and ACuCr4-III were considered for comparison.

The surface acidity expressed as DAS values increased upon impregnating 0.132 mole% chromia into Al–Cu–O system. Further increase of chromia beyond 0.132 mole% led to a decrease of surface acidity. In accordance with *Tanabe* [34, 35], the acid sites on a mixed oxide system may be developed by charge imbalance of oxide constituents, where the coordination number of minor cation determined the net charge of the mixed oxide. The elevation of calcination temperature to 923 K caused a two-fold increase of acid site concentrations. This may be judged from the creation of new *Lewis* and *Brønsted* acid sites *via* the dehydration upon heating from 723 to 923 K. However, although the increase of calcination temperature up to 923 K created an additional surface acidity, the rise of calcination temperature higher than 923 K reduced the surface acid density to 67.8%. This finding agrees with an earlier report [36], which was described that the thermal treatment at higher temperatures could promote an extra hydrolytic decomposition of surface acidic groups and therefore result in a decrease of acid sites.

Cyclohexanol Conversion as a Test of Surface Acidity

The catalytic investigation recorded cyclohexene as dehydration product (DHD) and cyclohexanone from dehydrogenation reaction (DHG). It was earlier reported that the dehydration of cyclohexanol takes place over acid sites, while the dehydrogenation reaction needs basic/redox sites [37–44]. Inspection of Table 2 demonstrates an increase of DHD and S_{DHD}, upon increasing of both chromia content and DAS value. The further increase of chromia content was associated with a decrease of both DAS value and dehydration activity (Fig. 5). In agreement with literature, a higher dehydration of cyclohexyl alcohol was observed for those catalysts of higher acid amounts. However, the increase of surface acidity was associated with a decrease of surface basicity, thus the dehydrogenation activity increased. CuO was reported as one of the most active metal oxides in the dehydrogenation reaction [13]. This fact could be attributed to the formation of $CuCr_2O_4$ as laterally approved by XRD technique. The increase of Cr_2O_3 led to spillover of CuO from

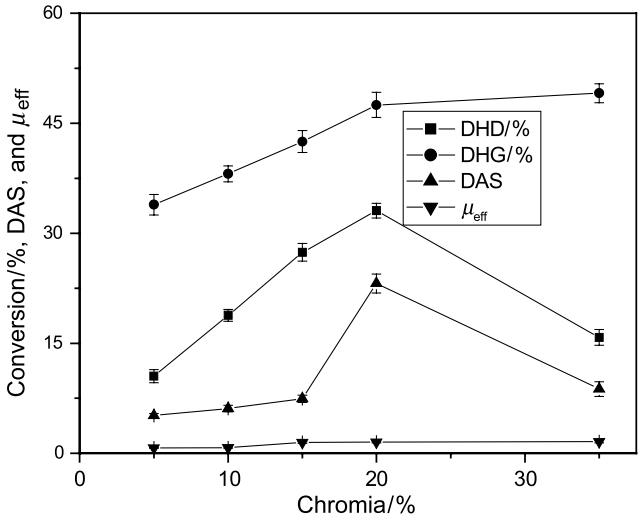

Fig. 5. Correlation between conversion, %, DAS, and μ_{eff} and chromia, %

the catalyst lattice matrix to form an additional $CuCr_2O_4$ species and therefore increased the dehydrogenation activity. As evident from Table 2, the values of μ_{eff} exponentially increase upon increasing the chromia content. Moreover, a direct correlation between μ_{eff} and DHG was found. The formation of $CuCr_2O_4$ as dehydration favoring spinel resulted in the increase of χ_m and thereby μ_{eff} *via* the cooperative effect of the aligned magnetism on the metal atoms, considering the contribution of Al_2O_3 in all samples.

This approach confirmed the importance of oxides' paramagnetism as catalysis criteria and evidently approved that the dehydrogenation of cyclohexanol occurred on redox centers. These findings indicated that *n*-butylamine non-aqueous titration and catalytic conversion of cyclohexyl alcohol could be used as a simple and rapid method in probing acid–base characteristics of solid catalysts [2, 11, 13, 45–47].

The rise of calcination temperature reduced the DHD and DHG activities as well as selectivities. In other words, thermal treatment beyond 923 K enhanced the elimination of surface OH groups (*M*–OH) and destructed thus some of the surface's acid–base nature [2, 15]. Moreover, the sintering phenomena led to a decrease of surface area accessible for the reactant molecules.

Reaction Mechanism

syn-Elimination of cyclohexanol was geometrically favored for the dehydration reaction, since the neighboring OH and H departing groups were coplanar. The reaction took place *via* the un-concerted mechanism, involving formation of a carbocation on *Brønsted* acid sites (Scheme 1).

In contrary, the dehydrogenation reaction occurred through a redox cycle owing to the mechanism shown in Scheme 2, where DHG reaction may take place on hydride accepting sites (metal cation as *Lewis* acid) and oxygen atom of basic nature (*Lewis* base).

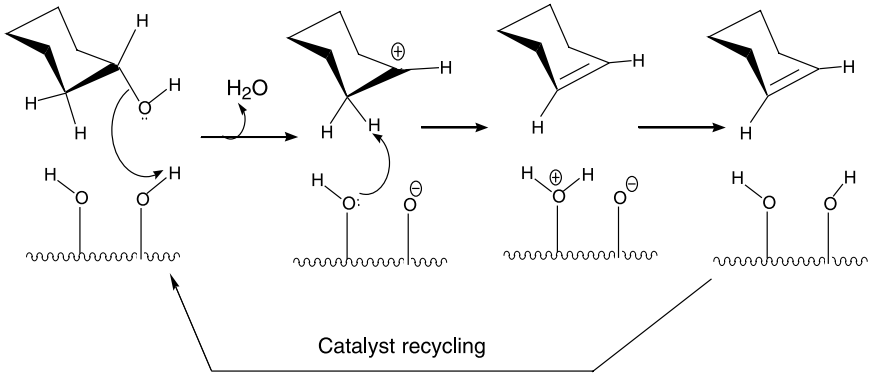

Scheme 1

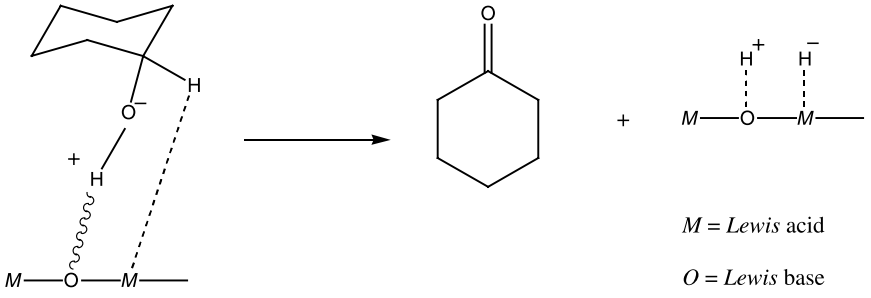

Scheme 2

Conclusions

The above results and discussions show that: (i) the textural and structural properties affected both DHD and DHG reactions; (ii) DHD reaction took place on *Brønsted* acid sites, while DHG reaction took place on redox centers; and (iii) a good agreement between two alternative methods, amperometric titration and catalytic conversion of cyclohexyl alcohol as a model reaction for probing acid–base sites of investigated catalysts.

Experimental

Catalysts Preparation

All catalyst precursors, namely $Al(OH)_3$, $Cr(NO_3)_3 \cdot 9H_2O$, and $Cu(NO_3)_2$ were obtained from BDH chemicals. Five series of the investigated catalysts were prepared by the incipient wetness impregnation of $Al(OH)_3$ with $Cu(NO_3)_2$. For each preparation, an aqueous solution of $Cu(NO_3)_2$ was vigorously stirred with $Al(OH)_3$ for 24 h. The samples were dried using a rotatory evaporator, heated at 373 K for 24 h. The dried samples were soaked in $Cr(NO_3)_3 \cdot 9H_2O$ dissolved in a least amount of water for 24 h, followed by re-drying at 373 K. The samples were grinded and calcined in air at 723 (I), 923 (II), and 1123 K (III) for 8 h. The content of Cr_2O_3 was adjusted to 0.033 (1), 0.066 (2), 0.099 (3), 0.132 (4), and 0.230 mole%, while CuO content was maintained to 0.2 mole%.

The catalysts were designated, where the letter A denoted to alumina, the Arabic numbers represented Cr_2O_3 contents, and the roman numbers showed the calcination temperature, *e.g.* the

catalyst ACuCr1-I assigned the sample containing 0.033 mole% chromia and calcined at 723 K, while ACuCr4-III represented the catalyst calcined at 1123 K and containing 0.132 mole% of chromia.

Powder X-Ray Diffraction (XRD)

XRD patterns were recorded with a Philips diffractometers type 1390, using monochromatic Ni-filtered copper radiation ($\lambda = 1.5405$ Å) at 30 kV and 10 mA. The diffraction was scanned at a rate of 2° min^{-1} within the intervals of $2\theta = 12$–80°. Statistical method, applying *Scherrer*'s equation (Eq. (3)), enabled us to calculate the crystallite size, where d is the mean crystalline diameter, λ the X-ray wave length, k the *Scherrer* constant (0.89), $B_{1/2}$ the full width half maxima (FWHM) of the detected phase, and θ the diffraction angle.

$$d = \mathrm{k}\lambda/(B_{1/2}\cos\theta) \tag{3}$$

Magnetic Susceptibility Measurements

The magnetizations of prepared catalysts in terms of magnetic susceptibility (χ_g) were estimated using the conventional *Gouy* method. Magnetic susceptibility of the pre-calcined catalysts has been measured in a quartz cell of 0.3 cm diameter and 1–2 cm length, using a Mettler balance model HL 52.

The effective magnetic moment (μ_eff) and the values of magnetic susceptibility (χ_g) of the 923 K – calcination products were estimated from the magnetization values. Contribution of the mixed oxides to the experimental magnetic susceptibility (χ_m) can be expressed using Eq. (4) where the coefficients a, b, and c are the weight percentage of the individual components, neglecting the contribution of oxygen magnetism [21].

$$\chi_\mathrm{m} = \mathrm{a}\chi_\mathrm{g} + \mathrm{b}\chi_\mathrm{g} + \mathrm{c}\chi_\mathrm{g} \tag{4}$$

The determination of χ_m enabled to evaluate the effective magnetic moment at 311 K, owing to the relationship (Eq. (5)).

$$\mu_\mathrm{eff} = 2.084(\chi_m \cdot T)^{1/2} \tag{5}$$

Textural Properties Measurements

Surface characteristics, including surface area (S_{BET}), mean pore radius (r^-), total pore volume (V_T) and the pore volume distribution of calcined catalysts were determined from nitrogen adsorption at 77 K, using Quantachrome Nova Automated gas sorption system. Prior to the adsorption measurements, out-gassing the surface took place under a reduced pressure of 10^{-5} torr for 2 h at 473 K in order to remove the adhered water.

Surface Acidity Measurements

The total acidity of investigated catalysts was determined *via* the batch titration method, using *n*-butylamine as a probe base [22]. The electrode potential (mV) was recorded with Orion A 420 digital *pH* meter *versus* the added volume of titrant at a sequential rate of 0.2 cm^3 min^{-1}. Before carrying out the experiment, a weight of 0.1 g was activated in a vacuum oven at 473 K for 24 h. The cooled sample was soaked in 10 cm^3 of acetonitrile, agitated for 30 min and the suspension was titrated with the probe titrant. Equilibrium time of *n*-butylamine adsorption was established while recording a fixed mV value. The titration continued till the complete probing of all acid centers with the titrant and no significant changes of mV with further addition of *n*-butylamine could be recorded. The surface acid density (DAS) was estimated according to Eq. (6) where D, V, and M are the density (g/cm^3), the saturation volume required to poison all acid sites (cm^3), and M is the molar mass of *n*-butylamine, respectively.

$$\mathrm{DAS} = [D \times V \times \textit{Avogadro}\text{'s number}/M]/S_{BET} \tag{6}$$

Catalytic Conversion of Cyclohexanol

The catalytic reaction was performed in a micro-reactor (*i.d.* = 7 mm) containing 0.2 g of pre-calcined catalyst and attached directly to a chromatographic column of PY-Unicam GC to analyze the reaction out-flow within the temperature 773 K. For each run, 3 mm^3 cyclohexanol were injected in a steam of N_2 carrier gas at constant rate of flow (30 $cm^3\,min^{-1}$).

References

[1] Bensi HA (1957) J Phys Chem **61**: 970
[2] El–Sharkawy EA, Mostafa MR, Youssef AM (1999) Colloids Surf A **157**: 211
[3] Dragoi B, Gervasini A, Dumitriu E, Auroux A (2004) Thermochimica Acta **420**: 127
[4] Mohamed MM, Abu-Zied BM (2000) Thermochimica Acta **359**: 109
[5] Wang WJ, Chen YW (1991) Catal Lett **10**: 297
[6] Patil PT, Malshe KM, Kumar P, Dongare MK, Kemnitz E (2002) Catal Commun **3**: 411
[7] Furuta S, Matsuhashi H, Arata K (2004) Appl Catal A **269**: 187
[8] Tanabe K, Masui S, Nishizaki T (1970) J Res Inst Catal Hokkaido Univ **19**: 1
[9] Corma A, Rodellas C, Fornes V (1984) J Catal **88**: 374
[10] Borgna A, Sepulveda J, Magni SI, Apesteguia CR (2004) Appl Catal A **276**: 207
[11] El-Sharkawy EA (1998) Adsorption Sci Technol **16**: 193
[12] Turek W, Haber J, Krowiak A (2005) Appl Surf Sci **252**: 823
[13] Bezouhanova CP, Al-Zihari MA (1991) Catal Lett **11**: 245
[14] Radwan NRE, El-Sharkawy EA, Youssef AM (2005) Appl Catal **93**: 106
[15] Al-Hakam SA, El-Sharkawy EA (1998) Matt Lett **36**: 167
[16] Mao D, Lu G, Chen Q (2004) Appl Catal A **263**: 83
[17] Mekhemer GAH, Ismail HM (2004) Colloids Surf A **235**: 129
[18] El-Sharkawy EA, Al-Shihry Shar S, Ahmed AI (2003) Adsorption Sci Technol **21**: 863
[19] Huang Ta-Jen, Lee Kuen-Cheung, Yang Hsiao-Wen, Dow Wei-Ping (1998) Appl Catal A **174**: 199
[20] Zahran AA, Shaheen WM, El-Shobaky GA (2005) Mater Res Bull **40**: 1065
[21] Hierl R, Knozinger H, Urbach H (1981) J Catal **69**: 475
[22] Cid R, Recchi G (1985) Appl Catal A **14**: 15
[23] Mazzocchia C, Kaddouri A (2003) J Mol Catal A **204**: 647
[24] Chen HC, Gillies GC, Anderson RB (1980) J Catal **62**: 367
[25] Youssef AM, Ahmed AI, Al-Assy NB, Samra SE, El-Sharkawy EA (1995) Adsorption Sci Technol **12**: 335
[26] Brunaeur S, Deming LS, Deming WE, Teller A (1940) J Am Chem Soc **62**: 1723
[27] Gregg SJ, Sing KSW (1982) Adsorption Surface area and porosity, 2nd edn. Academic Press, London
[28] Sing KSW (1982) Pure Appl Chem **54**: 2201
[29] Ahmed AI, El-Nabarawy Th (1985) Surf Technol **26**: 225
[30] Mostafa MR, Youssef AM (1994) Materials Lett **18**: 273
[31] Ghonem NM, El-Nabarawy Th, Morsei IM, Amin NH (1988) Bull NRC Egypt **13**: 11
[32] El-Shobaky GA, El-Khouly SM, Ghozza AM, Mohamed GM (2006) Appl Catal A **302**: 296
[33] Turky AM, Radwan NRE, El-Shobaky GA (2001) Colloids Surf A **181**: 57
[34] Tanabe K (1985) Catalysis by Acids and Bases. In: Imelik B, Naccache C, Coudurier G, Ben Taarit Y, Vedrine JC (eds) Elsevier Amsterdam
[35] Tanabe K (1989) New Solid Acids and Bases. In: Tanabe K, Misono M, Ono Y, Hattori H (eds) (Kodansha/Elsevier, kyo/Amsterdam **51**: Ch 3
[36] Samra SE, Youssef AM, Ahmed AI (1990) Bull Soc Chim Fr **127**: 174

[37] Valento A, Lin Z, Brandao P, Portugal I, Anderson M, Rocha J (2001) J Catal **200**: 99
[38] Bezouhanova CP, Al-Zihari MA (1991) Catal Lett **11**: 245
[39] Jonstone RAW, Liu J, Whittaker D (1998) J Chem Soc Perkin Trans **2**: 1287
[40] Jonstone RAW, Liu J, Whittaker D (2001) J Mol Catal A **174**: 159
[41] Fridman VZ, Davydov AA (2000) J Catal **195**: 20
[42] Liu Z, Xu Z, Yuan Z, Lu D, Chen W, Zhou W (2001) Catal Lett **75**: 203
[43] Nur H, Hamdan H (2001) Mater Res Bull **36**: 315
[44] Reddy BM, Ganesh I (2001) J Mol Catal A **169**: 207
[45] Bautista FM, Campelo JM, Garcia A, Luna D, Marinas JM, Garcia JI, Mayoral JA, Pires E (1996) Catal Lett **36**: 215
[46] Bautista FM, Campelo JM, Garcia A, Luna D, Marinas JM, Moreno MC, Romero AA (1998) Appl Catal **170**: 159
[47] Costa MCC, Hodson LF, Johnstone RW, Liu JY, Whittaker D (1999) J Mol Catal A **142**: 349